THE ASTROPHYSICAL JOURNAL, 474:188–204, 1997 January 1
© 1997. The American Astronomical Society. All rights reserved. Printed in U.S.A.

HUBBLE SPACE TELESCOPE OBSERVATIONS OF PLANETARY NEBULAE IN THE MAGELLANIC CLOUDS. V. MASS DEPENDENCE OF DREDGE-UP AND THE CHEMICAL HISTORY OF THE LARGE MAGELLANIC CLOUD

M. A. DOPITA,[1,2] E. VASSILIADIS,[3,4] P. R. WOOD,[1] S. J. MEATHERINGHAM,[1] J. P. HARRINGTON,[5]
R. C. BOHLIN,[3] H. C. FORD,[3] T. P. STECHER,[6] AND S. P. MARAN[6]
Received 1996 March 11; accepted 1996 July 17

ABSTRACT

A photoionization analysis of *Hubble Space Telescope* UV and ground-based optical spectrophotometry is given for eight more planetary nebulae (PNs) in the Large Magellanic Cloud (LMC). This allows the central stars to be placed accurately on the H-R diagram and permits the determination of the He, C, N, O, Ne, S, and Ar abundances. In some cases, the gas-phase abundances of Mg and Si may also be determined. We have combined these results with the analysis of two other objects published by us in the first two papers of this series. The observed abundance patterns are qualitatively consistent with the (mass-dependent) operation of the various chemical dredge-up processes as predicted by theory. Dredge-up of C during the thermal pulsing stage appears to be most important, and "hot bottom burning" transforms much of this C to N in the more massive stars. There is no sign of dredge-up of ^{22}Ne. We show that the spread in the α-process element abundances can be understood as being due to differences in core mass of the planetary nebula nucleus, which is related directly to initial mass of the precursor star. This is, therefore, a tracer of the age-metallicity relationship for stars in general, and we derive, for the first time, the chemical history of the LMC based on PNs. We find that the base metallicity of the LMC almost doubled $\sim$2 Gyr ago. This is consistent with studies of field stars and of clusters that show that there was a major burst of star formation at that time.

Subject headings: galaxies: abundances — galaxies: Magellanic Clouds — planetary nebulae: general — stars: evolution

1. INTRODUCTION

The planetary nebula (PN) phase of evolution represents the final phase of late stellar evolution of low- to intermediate-mass stars as they pass on their way to becoming white dwarfs. During the asymptotic giant branch (AGB) phase that precedes the PN phase, there occurs a complex series of thermal-pulsing events, chemical processing, and dredge-up into the envelope, accompanied by rapid and episodic mass loss. This is terminated by a final envelope ejection event that may, or may not, be correlated with the phase of the He-flash cycle. All these processes affect the subsequent evolution in the PN phase and are still relatively poorly understood, although rapid theoretical progress into these questions has been made in recent years (Schönberner 1983; Weidemann 1987; Alongi et al. 1993; Vassiliadis & Wood 1993; Bressan et al. 1993; Chiosi & Marigo 1996).

In our major *Hubble Space Telescope* (*HST*) program, results of which were reported in the first four papers of this series (Dopita et al. 1993, 1994, 1996, hereafter Papers I, II and IV, respectively; Vassiliadis et al. 1996, hereafter Paper III, we have circumvented the distance scale problem that plagues studies of Galactic PNs by investigating a sample of PNs in the Magellanic Clouds (MCs) drawn from the catalog of Sanduleak, MacConnell, & Davis Philip (1978). At optical wavelengths, this population has already been the subject of a systematic and detailed observational study both by us and by the University College group. Data on the line fluxes, the nebular densities, the expansion velocities, and the kinematics have all been accumulated in the last few years (see the review by Barlow 1989; also Dopita et al. 1985, Dopita, Ford, & Webster 1985; Meatheringham et al. 1988a, Meatheringham, Dopita, & Morgan 1988b, Wood, Bessell, & Dopita 1986, Wood et al. 1987, and Jacoby, Ciardullo, & Walker 1990). The distance to the MCs has been established accurately by a variety of other techniques (among which determinations based upon Cepheid variables, and upon SN 1987A, are the most accurate).

At the distance of the LMC, the PNs typically subtend less than 1″ on the sky. Nonetheless, they remain well resolved by the *HST*, and fine details of their internal structure may often be distinguished (Dopita et al. 1996). In addition, they typically display low systemic reddening. This is particularly important for their spectroscopic study in the UV, where we can not only detect directly the central star through its continuum and absorption line system, but we can also use the nebular spectrum to determine directly the chemical abundances of many elements that are not accessible to analysis either at optical or IR wavelengths. In particular, we can observe all the elements thought to be involved in dredge-up chemical processing; He, C, N, and O. In many respects, therefore, the LMC and SMC PNs represent a key to our understanding of the details of evolution beyond the AGB.

The results of the FOS spectroscopy of these objects has already been given by Vassiliadis et al. (1996). Here we present detailed photoionization models for individual objects, which allows us to infer observationally details of

[1] Mount Stromlo and Siding Spring Observatories, Institute of Advanced Studies, Australian National University, Private Bag, Weston Creek P.O., ACT 2611, Australia.
[2] Michael.Dopita@anu.edu.au.
[3] Space Telescope Science Institute, 3700 San Martin Drive, Baltimore, MD 21218.
[4] Currently at Instituto de Astrofisica de Canarias, Via Lactea, E-38200, La Laguna, Tenerife, Canary Islands, Spain.
[5] Department of Astronomy, University of Maryland, College Park, MD 20742-2421.
[6] NASA Goddard Space Flight Center, Greenbelt, MD 20771.

the operation of the chemical dredge-up processes, and which gives us first results on the chemical evolution of the Large Magellanic Cloud as a whole.

The distance to the LMC is assumed to be 50 kpc in the analysis that follows. This now appears to be well established through a number of techniques. From Cepheid period-luminosity (PL) and period-luminosity-color (PLC) relations, distance modulii of 18.4–18.55 are obtained (Caldwell & Laney 1991). An analysis of the ionization of the ring in SN 1987A gave a modulus of 18.5 (Panagia et al. 1991). Finally, an extremely accurate distance modulus has been determined by fitting theoretical light curves to a bump Cepheid in the LMC. This gives 18.53 ± 0.04 (Wood, Arnold, & Sebo 1996). Any systematic error in the assumed distance will propagate to all luminosities quoted, and this will in turn affect systematically estimates of core mass, initial mass, and age of the central stars.

2. PHOTOIONIZATION MODELING

The UV spectrophotometry (Vassiliadis et al. 1996) was combined with ground-based data (Meatheringham & Dopita 1991a, 1991b) to generate a self-consistent set of de-reddened line intensities extending from 1216 Å to beyond 7300 Å in the red. These spectra are interpreted in conjunction with the *HST* imaging data using the generalized modeling code MAPPINGS II (Binette, Dopita, & Tuohy 1985; Sutherland & Dopita 1993). The goals of this self-consistent nebular modeling are as follows:

1. As far as possible, match the modeled size, density, and internal structure of the nebula with observations.
2. Determine a luminosity of the central star that agrees with both the absolute luminosity of the nebula and the observed continuum flux, particularly in the UV.
3. Find the temperature of the central star and the strength of the local UV field (the ionization parameter) that matches the observed degree of ionization and excitation.
4. Determine the chemical abundances for each element in the nebula (the "metallicity") that matches the observed line spectrum as closely as possible.
5. Determine whether, and to what extent, the nebula leaks UV radiation (optically thin or thick).

Extremely valuable constraints can be obtained from the *HST* imaging data. For all the PNs for which we have spectra, we had earlier obtained (Dopita et al. 1996) Planetary Camera (PC) images in the [O III] λ5007 line, chosen because it is generally the brightest emission line in the optical. These images provide both size and structural information that can be used as input to detailed photoionization modeling analysis.

From the analysis of a sample of 15 planetary nebulae in the Magellanic Clouds, Dopita et al. (1996) found clear evidence for size evolution across the H-R diagram. However, the younger, low-excitation, compact PNs tend to be systematically smaller than photoionization models based on ground-based data would predict, suggesting these have a central reservoir of dense atomic and molecular gas. This gas lies close to the central star and is currently undergoing ionization and being accelerated into outflow. PNs classified previously as nitrogen-rich objects with massive central stars (Peimbert type I) show mostly the bipolar "butterfly" symmetry that is also a characteristic of their Galactic counterparts.

The derived kinematic ages range from less than 1000 yr up to almost 5000 yr but show little sign of systematic increase along the evolutionary tracks. Overall, the lack of any clear correlation of dynamical age and position on the H-R diagram seems to result from the dynamical evolution of the PN nebular shells themselves, the details of which also depend upon whether the central star leaves the AGB as an H or He burner. A correlation between the excitation class and expansion velocity was found by Dopita et al. (1988). In its turn, excitation class is correlated closely with the logarithm of the effective temperature (Dopita & Meatheringham 1991a). Subsequently Dopita (1993) found that an even better correlation existed between a combination of $\log(L/L_\odot)$, $\log(T_{\rm eff})$, and expansion velocity:

$$(V_{\rm exp}/{\rm km\ s^{-1}}) = -128 \pm 4 + 38 \pm 2 \times [\log(T_{\rm eff}) - 0.25 \pm 0.05 \log(L/L_\odot)] .$$

The true ages of the larger objects are therefore systematically underestimated because of acceleration of the nebular shell during its lifetime. Apparently the PN shells are accelerated initially by the increase of thermal energy content during their nuclear burning phase of evolution and coast at almost constant expansion velocity during the fading track. In this model, the stellar wind provides the pressure that confines the ionized material to a (somewhat) thin shell. The terminal velocity reached by the nebular shell is correlated with the mass of the PNs, with more massive PNn's driving faster expansion. The increase in thermal energy content is due in part to the temporal increase in ionized mass, but is mostly due to thermalization of the fast stellar wind, which develops as the PNn tracks to high temperature on the H-R diagram.

Using the $V_{\rm exp}$:$\log(T_{\rm eff})$:$\log(L/L_\odot)$ relation, along with the Vassiliadis & Wood (1993) theoretical evolutionary tracks of the central star, Dopita et al. (1996) derived two semiempirical estimates for the evolutionary timescales based upon the nebular size and the measured dynamical age. They then demanded that these evolutionary timescales should be consistent with the evolutionary age derived from theory. With this assumption, they concluded that He-burning PNn's outnumber the H burners in the approximate ratio 2:1 in the LMC.

2.1. *The Nebular Density Model*

The essential features of the imaging data summarized above provide the basis for the nebular density model that we have adopted. This model must be reasonably physical, but it must also be fairly simple so that the nebular parameters can be well constrained by the available observational material. Clearly, the features of the dynamical and size evolution support the "interacting winds" model of Kwok, Purton, & Fitzgerald (1978) in which a fast ($V > 100$ km s^{-1}) wind interacts with much slower ejecta ($V \sim 10$ km s^{-1}) ejected during the AGB. The fast wind both ionizes and sweeps out the slow-moving ejecta. Provided either that the slow-moving ejecta were ejected with nonspherical symmetry, or that instabilities in the interaction with the fast wind has allowed the slow-moving ejecta to be broken up into clumps at a characteristic radius, the photoionization model can be simplified to a two-zone model, one dealing with the material close to the clumps, and the other describing the (lower density) ionized flow region. Both these components are necessary in order to produce a satisfactory photoionization model, as we found in the first two papers of this series (Dopita et al. 1993, 1994).

In our fitting procedure, therefore, we have adopted mostly a two-zone model. Zone 1 is an optically thick, isobaric region having a certain covering factor as seen at the central source. This region is ram-pressure confined at its inner boundary by the standoff shock in the fast wind of the PNn, and it will produce the bulk of the emission in lines of low-ionization potential, which are produced close to ionization fronts. The density in this region is therefore well constrained by electron densities inferred from the [S II] or [O II] density-sensitive line ratios.

Zone 2 is a region with density law of the form $n_H(R) = A + BR^{-2}$, which covers the remainder of the solid angle as seen at the central source. This region may be either optically thick or thin. The rationale behind this choice is that since there is an ionization front eating into the store of neutral gas ahead of zone 1, there is a continuous supply of gas available to be photoionized and accelerated into the surrounding space either through its own pressure gradient or with the assistance of the ram pressure of the fast stellar wind. This sets up a density distribution that is decreasing steeply in the radial direction. The *HST* nebular photometry (Dopita et al. 1996) indicates this to be the case for those objects that are well resolved. However, in the outermost regions, the density will tend to become approximately constant with the pressure of the ionized gas being determined by the ram pressure of the stellar wind at the mean radius of the stellar wind shock, which generally will lie well outside the inner edge of zone 1. Since the fast wind that is accelerating the nebular shell originates at the central star, we assume also that the radii of the inner boundaries of both zones are the same. To allow the flow to escape from the region of the ionization front, the inner density of zone 2 must be always lower than that of zone 1. The radius of the inner boundary of the nebular shell is inferred from inspection of the nebular morphology, in the cases in which this is possible.

2.2. *Derivation of Stellar Parameters*

The first object of nebular modeling is to be able to place the central star of the PN upon the Hertzsprung-Russell (H-R) [log L: log ($T_{\rm eff}$)] diagram. For the hot central stars of PNs, by far the greatest fraction of the energy is put out below the Lyman limit. In an optically thick nebula, in which the ionizing radiation from the central star is totally absorbed, the luminosity is directly proportional to the sum of all the nebular emissions (line, continuum, and IR). This is the principle of the "energy balance" concept. This technique, discussed first by Stoy (1933) and improved by Kaler (1976) and Priete-Martinez & Pottasch (1983), can also be used to derive the effective temperature of the central star, since the mean energy per photoionization becomes larger for hotter stars, so there is a direct correlation between the nebular and the stellar temperature. This method, extremely accurate in principle, is often difficult to apply, since it depends on having a complete set of measurements of the nebula. It has most notably been applied by Ratag (1991) in the context of the Galactic bulge population of bright PNs.

For PNs in the Magellanic Clouds, prior to *HST* we usually had available only optical spectrophotometric measurements. Photoionization modeling of the PNs (Dopita & Meatheringham 1991a, 1991b) had therefore to rely mainly on the Hβ flux (as a measure of the recombinations, and therefore of the ionizing flux) to derive the luminosity of the central star, and upon the degree of excitation of the nebula (which is related to the ionization temperature of the central star) to estimate the temperature of the central star. The main problem with this is that many PNs absorb the UV radiation completely in some directions, but are very optically thin in other directions. From ground-based data alone, the optically thin portions may contribute little to the total flux, and they often contribute significantly only to lines of high ionization potential, which are not the main coolants in the optical. Nebular modeling based on optical spectra alone will in general lead to an underestimate of the luminosity, and, to a lesser extent, it will provide an overestimate of the temperature of the central star.

The HST spectral data provides vital complementary data for our understanding of the distribution of PNs on the H-R diagram, and for their dynamical and physical evolution. From the spectral distribution in the continuum, in many cases we can detect directly the central star at far-UV wavelengths. In one or two cases, we can even measure the line profiles produced in the atmosphere of the central star to estimate stellar wind parameters. For a blackbody stellar source in the LMC, the apparent brightness (ergs cm^{-2} s^{-1} Å^{-1}) at the edge of the Earth's atmosphere at wavelength λ(Å) is given by

$$B(\lambda) = \frac{4.956 \times 10^{-19}(R/\mathrm{cm})^2(\lambda/\text{Å})^{-5}}{\{\exp\,[1.439 \times 10^8(\lambda/\text{Å})^{-1}(T/\mathrm{K})^{-1}] - 1\}}\,, \quad (2.1)$$

where R is the radius of the star, and T is its effective temperature. This formula can be used to determine the luminosity of the star directly.

In an optically thick PN, the ratio of stellar to nebula continuum intensities gives a direct estimate of the effective temperature of the central star, and in the UV we can detect many resonance and intercombination lines of highly ionized species that are sensitive to the optically thin regions of the nebula, allowing these estimates to be corrected for the escape of UV photons from the nebula.

2.3. *Self-consistent Photoionization Models*

With the density model presented above, we proceed with photoionization modeling in the manner already described in Dopita et al. (1993, 1994). Our MAPPINGS II photoionization models must match the observed linear size, morphology, densities determined from [O II], [S II], or the UV lines, and the reddening-corrected Hβ flux. The central star is assumed to have a blackbody distribution in frequency. Stellar and nebular parameters and chemical abundances of each element are changed by hand at each iteration until the dispersion of the observed versus theoretical line intensities is minimized for all ionization stages of each element. In this procedure, the overall degree of excitation is determined largely by the assumed effective temperature of the central star. Typically four or five iterations are required until a satisfactory model is obtained. For most objects, unless otherwise noted, the random errors in the abundances of individual ions may be as large as $\pm 25\%$, but random errors in the abundances of individual elements are mostly only $\pm 15\%$, since these are determined by the error in the mean abundance of the dominant ionization stages, which are smaller than the errors associated with minor ionic constituents.

Some lines prove to be quite sensitive to the degree of optical thinness. In particular, strong He II, [N V], [Ne V], and [Ne IV] lines frequently show the need for an optically thin component, as do weak C II], [N I], [N II], [O I], or [O II] lines. These lines provide very useful constraints on the parameters of both zones. In Figure 1 we show separa-

tely the contributions of the two components for one object (LMC-SMP 8) that displays both optically thick and optically thin components. The requirement for the contributions of both components to ensure the goodness of fit is clearly indicated. The discussion on the fits for individual objects in § 2.4 expands this point.

For cooler objects, the central star is directly visible through its UV continuum. For our final models of each object, we have constructed the theoretical nebular continuum and added to this the predicted stellar continuum predicted by equation (2.1). A comparison with the observed continuum always provides a "sanity check" of the model, and in some cases it also allows us to obtain an independent estimate of the luminosity of the central star, provided we assume that the temperature of the central star has been determined accurately from the nebular model. An attempt to determine directly the temperature from a variant of the classical Zanstra method would often be invalidated by the optical thinness of zone 2 of the model.

The parameters estimated for each of the models are given in Table 1. The derived elemental abundances for these models, and for those of Papers I and II, are given in Table 2. The detailed spectral model fits are given in Table 3, and the goodness of fit of the spectral line model is shown in Figures 2*a*–2*b*. Model continuum fits for objects in which the central star is detectable are given in Figures 3*a*–3*c*. Finally, Table 4 gives the logarithmic abundances with respect to the solar values from Anders & Grevesse (1989) in accordance with the usual practice of stellar spectroscopists. We have used the mean of the heavier α-process element abundances with respect to the solar values

$$[\alpha/\mathrm{H}] = ([\mathrm{Ne/H}] + [\mathrm{S/H}] + [\mathrm{Ar/H}])/3 \qquad (2.2)$$

as our "metallicity" indicator. These elements are less likely to be affected by dredge-up processes (see the discussion in § 3.4, below). Such an average reduces the uncertainty in the abundance with respect to the solar values. In Tables 2 and 4 we have also added the results for LMC-SMP 83 and LMC-SMP 85 from Papers I and II of this series (Dopita et al. 1993 and 1994).

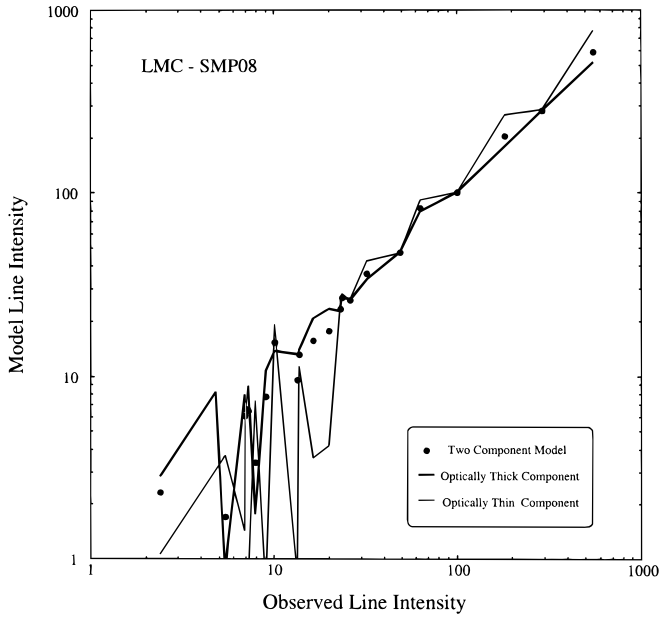

FIG. 1.—The theoretical line fit for LMC-SMP 8 showing the contributions made by each of the zones of the photoionization model, showing clearly the need for both an optically-thick and an optically thin component.

It is useful to conclude this section with a few remarks about temperature-sensitive lines such as [O III] λ1363. In general, observers spend a great deal of effort measuring such lines in order to determine the nebular temperatures. However, temperature-sensitive lines such as this one are enormously affected by fluctuations in the temperature, as has been pointed out many times over the years by the Peimberts and their coworkers (see the recent review by Peimbert (1995), and references therein). Any temperature enhancements that are due to shock waves and turbulence, or any temperature enhancements near ionization fronts, will enhance the intensity of such lines, leading to an overestimate of the mean temperature, and in consequence, an underestimate of the elemental abundances. To quote from that paper "... the best determinations of abundance ratios are those that do not depend, or depend weakly, on the electron temperature." In this sense, the self-consistent global modeling that we present here should approach this ideal since we seek simply to minimize the scatter between the observed and modeled intensities of all lines on a logarithmic plot, without any regard to temperature or correction for unseen stages of ionization. However, it should be remarked that this procedure is only made possible by the fact that we have both the UV and visible spectra, which permit a good determination of the abundances of all of the important coolants in the nebula.

2.4. *Notes on Individual Objects*

2.4.1. *LMC-SMP 2*

This PN is a rather faint, low-excitation object (excitation class EC = 1.1) with low expansion velocity (9.9 km s^{-1}). The *HST* image shows it to be a fairly compact object with a steep radial density distribution. The central star is strongly detected in the UV with deep C IV absorption and other absorption lines visible. It is also detectable at optical wavelengths against the nebular continuum.

The weak C II], [S II], and [N II] lines all indicate that this PN is optically thin. The [O II] density has not been measured directly, but the relative strengths of the [O II] λλ7320,7330 and λλ3727,3729 lines indicate that the density in the outer parts must be quite low.

An adequate fit is obtained with zone 2 only. The stellar luminosity is quite low. The nebular model gives $L = 1345 \pm 200\ L_\odot$, while a fit to the nebular continuum would yield $L = 1500 \pm 300\ L_\odot$. This implies a low-mass, old central star.

2.4.2. *LMC-SMP 8*

This PN is a low-excitation object (EC = 2.5) with moderate expansion velocity (25 km s^{-1}). The absence of [S II] and the weakness of the [N II] lines in the red suggest optical thinness and/or high density. The ratio of the [O II] λλ7320,7330 and λλ3727,3729 lines would require a very high density, but the ratio of the near-UV lines of [O II] λλ3727/3729 indicates a density of only 5500 cm^{-3}. The only way to reconcile these is to have two components. One of these must be very dense and compact, and the other must be much less dense in the outer regions, but very much more extended to provide the required emissivity. This is consistent with the appearance of the *HST* image, which strongly suggests a core + halo structure.

The fit to the continuum yields an extraordinary result.

TABLE 1

SUMMARY OF TWO-ZONE NEBULAR MODELS FOR THE LMC PNs

OBJECT	STELLAR PARAMETERS			NEBULAR PARAMETERS (ZONE 1)				NEBULAR PARAMETERS (ZONE 2)				
	$L/L_\odot$	$L_{UV}/L_\odot$	$T_{eff}/10^4$ K	n(H) (cm^{-3})	R_{in} (cm)	R_{out} (cm)	Coverage Factor	B (cm^{-1})	A (cm^{-3})	R_{in} (cm)	R_{out} (cm)	τ_{out}
LMC-SMP 02.....	1345 ± 150	1500 ± 300	3.9 ± 0.15	...	...	...	...	25000	1600	2.00E+16	1.72E+17	3.05
LMC-SMP 08.....	3930 ± 300	(See text)	5.2 ± 0.40	120000	2.00E+16	3.04E+16	0.29	20000	2000	2.00E+16	1.85E+17	0.79
LMC-SMP 20.....	3300 ± 300	...	15.1 ± 0.8	1000	1.00E+17	4.01E+17	0.73	2000	2300	8.00E+16	2.93E+17	...
LMC-SMP 35.....	2405 ± 800	...	10.8 ± 0.8	2900	2.50E+17	3.58E+17	0.16	1000	600	2.50E+16	5.52E+17	7.8
LMC-SMP 40.....	1330 ± 250	...	17.6 ± 0.7	1600	1.70E+17	3.60E+17	0.50	850	...	1.80E+17	3.83E+17	11.2
LMC-SMP 47.....	4750 ± 200	...	14.1 ± 0.5	16000	4.00E+16	1.27E+17	0.50	6500	...	8.00E+16	2.29E+17	...
LMC-SMP 76.....	5432 ± 300	5500 ± 500	5.8 ± 0.30	100000	2.78E+16	3.97E+16	0.20	40000	10000	2.50E+16	1.18E+17	...
LMC-SMP 87.....	4900 ± 400	...	16.8 ± 0.5	3500	3.60E+17	4.09E+17	0.45	1000	...	1.50E+17	3.86E+17	2.5

TABLE 2

SUMMARY OF ABUNDANCE DETERMINATIONS FOR LMC PNs[a]

Object	He	C	N	O	Ne	Mg	Si	S	Ar
LMC-SMP 02.....	11.01	8.57	7.36	8.26	7.45	...	...	6.60	6.00
LMC-SMP 08.....	11.28	7.93	7.48	8.26	7.32	...	...	6.69	6.04
LMC-SMP 20.....	11.15	7.52	8.58	8.49	7.74	...	7.52	7.26	6.34
LMC-SMP 35.....	10.95	8.53	7.78	8.38	7.48	...	6.78	6.70	5.93
LMC-SMP 40.....	11.01	8.81	7.79	8.45	7.65	6.11	...	6.79	5.83
LMC-SMP 47.....	11.24	8.18	8.15	8.36	7.60	6.20	6.52	6.85	6.28
LMC-SMP 76.....	10.88	9.04	7.40	8.30	7.34	...	...	6.60	5.90
LMC-SMP 83.....	11.11	7.41	8.06	8.62	7.71	...	...	7.38	6.45
LMC-SMP 85.....	11.02	8.74	7.63	8.40	7.48	...	...	6.30	6.24
LMC-SMP 87.....	11.25	7.90	8.95	8.56	7.90	...	6.90	7.11	6.18
⟨LMC⟩[b]	10.95	8.04	7.14	8.35	7.61	7.47	7.72	6.81	6.29

[a] Given in terms of $12.0 + \log(x/\mathrm{H})$.
[b] Taken from Russell & Dopita 1992.

The stellar continuum that is observed is completely inconsistent with the luminosity of $3930 \pm 300\ L_{\odot}$ inferred from the nebular model. At 1300 Å, the observed stellar continuum is about 20 times too weak. Furthermore, there is a pronounced 2200 Å absorption feature in the continuum. Therefore, we must conclude that the central star is heavily reddened compared with the nebula. This could occur if the dense reservoir of dusty neutral gas was obscuring the central star, but not the ionized gas. The strength of the 2200 Å feature is inconsistent with an LMC reddening law (Fitzpatrick 1985) for this dust, and even a Galactic reddening law (Seaton 1979) with a logarithmic reddening constant, $c = 0.48$, can hardly reproduce the depth of the 2200 Å feature (see the resulting continuum fit in Fig. 3).

This result proves that the dust ejected by PNs can be a carrier of the 2200 Å feature. The most likely explanation of the feature is that it results from a surface "charge slop" resonance on very small carbon spheres or shells, possibly even on C_{60} Buckminsterfullerene (see the discussion in Hoyle & Wickramasinghe 1991). Such C-rich dust is likely to be ejected during the carbon star phase. However, the abundance analysis for this particular PN shows it not to be particularly C-rich. This may simply reflect the fact that photodestruction of C-bearing grains has not yet had a chance to occur, given the extremely high density and the youth of this nebula.

2.4.3. *LMC-SMP 20*

This PN is a fairly large ($D \sim 0.2$ pc) bipolar, high-excitation (EC = 8.1) type I object. The accuracy of the modeling was affected somewhat by the loss of lock event, which caused the G130H exposure to fail. Nonetheless, a quite satisfactory fit could be obtained using only the portion of the spectrum that remained. The nitrogen abundance is likely to be somewhat less accurate for this object, since the N IV] and the N V lines were not observed, and these are dominant ionization states.

2.4.4. *LMC-SMP 35*

This PN is a large ($D \sim 0.3$ pc) shell-like intermediate-excitation object (EC = 5.4) with a high expansion velocity (41 km s^{-1}). At 1".2 diameter, it is appreciably larger than the 1".0 FOS aperture, so that only about 40% of the total flux is collected in the UV (Vassiliadis et al. 1996). As a consequence, it is very difficult to model, since the UV spectrum samples a different region of nebula than does the optical, which accepts all the nebular light. These calibration problems are apparent in the region of the Balmer jump, which is too deep in the merged spectrum. The UV lines appear to be overestimated with respect to the optical by a factor of order 1.6.

From the scatter in the model versus observed line intensities, we estimate the errors in the abundances to be ~30% for this object.

2.4.5. *LMC-SMP 40*

This PN is a fairly large ($D \sim 0.2$ pc) high excitation (EC = 7.6) object with a very clear distorted ring morphology and a high expansion velocity (54 km s^{-1}). A simple, optically thick isobaric model provides a fairly good description of the observed spectrum. However, this model overestimates the strengths of [O I] and [N I], underestimates the C IV/C III] ratio, and predicts the [Ne V] lines far too weak. It is clear, therefore, that a substantial contribution of optically thin gas is required, and that the object is probably a bipolar PN seen almost pole-on. This would provide a natural explanation for the rather high expansion velocity. Given the large inner radius, we adopted an isochoric density law for zone 2.

2.4.6. *LMC-SMP 47*

This PN is a compact bipolar type I object with moderate excitation (EC = 6.8) and a very high expansion velocity (79 km s^{-1}). It proved to be very easily modeled, and an isobaric optically thick component by itself gave a good description of the model. However, we adopted a model with two optically thick isobaric components of different densities and inner radii to improve the fit to the observed image morphology.

2.4.7. *LMC-SMP 76*

This PN is very compact with low excitation (EC = 2.6) and moderate expansion velocity (29 km s^{-1}). The central star is strongly detected, along with a number of stellar absorption lines. The C IV line displays a pronounced P Cygni profile. The nebula is characterized by a very high C abundance, as was inferred by Vassiliadis et al. (1996). The luminosity inferred from the photoionization model and from the stellar UV continuum agree well with each other.

2.4.8. *LMC-SMP 87*

This is a very large ($D \sim 0.25$ pc) optically thin type I PN of very high excitation (EC = 9.0). It proved very difficult to model because the PN is larger than the FOS and therefore, as for LMC-SMP 35, there is a mismatch between the UV and optical spectra. The extreme intensity of the N V, N IV],

TABLE 3

OBSERVED AND MODEL FLUXES FOR LMC PLANETARY NEBULAE

		LMC-SMP 02		LMC-SMP 08		LMC-SMP 20		LMC-SMP 35	
λ (Å)	LINE IDENTIFICATION	Observed $\log L(\mathrm{H}\beta) = 34.33$	Model $\log L(\mathrm{H}\beta) = 34.4$	Observed $\log L(\mathrm{H}\beta) = 34.97$	Model $\log L(\mathrm{H}\beta) = 35.00$	Observed $\log L(\mathrm{H}\beta) = 34.72$	Model $\log L(\mathrm{H}\beta) = 34.70$	Observed $\log L(\mathrm{H}\beta) = 34.72$	Model $\log L(\mathrm{H}\beta) = 34.70$
1239, 1243...	N v	...	...	...	...	...	428.2	...	...
1336	C II	...	...	7.2	6.5	...	...	9.7	20.7
1483	N IV]	...	...	...	...	...	...	8	5.0
1548	C IV	...	...	7.9	3.4	...	...	282	123.2
1551	C IV	...	...	5.4	1.7	...	...	196	62.5
1640	He II	...	...	...	...	494	519.1	...	...
1661	O III]	...	...	...	...	13.3	10.4	18.2	7.3
1666	O III]	...	...	...	...	43.9	25.5	26.4	17.7
1740, 1742...	N III]	...	...	...	...	214	176.0	11	20.7
1884	Si III]	...	...	...	...	30.3	14.9	...	...
1892	Si III]	...	...	...	...	14.2	17.0	8.4	9.2
19079	C III]	128	116.6	63.4	81.9	111	91.8	558	636.0
2139	N II]	...	...	...	...	28.3	15.0	...	...
2321, 2325...	[O III], C II]	19.1	32.8	16.4	15.7	...	...	...	...
2424	[Ne IV]	...	...	...	...	160.7	122.9	54.6	...
2470	O II]	8.5	6.2	...	...	10.2	6.7	...	9.3
3343	[Ne V]	...	...	...	...	27	16.8	8.3	...
3426	[Ne V]	...	...	...	...	76	44.2	14.4	...
3727, 3729...	[O II]	180.4	140.4	10.1	15.3	141.2	132.1	84.2	120.8
3869	[Ne III]	...	...	32.2	36.2	109.6	123.7	79.2	80.5
3969	[Ne III], Hϵ	15.7	29.8	23.7	27.0	50.7	50.3	43.8	40.0
4069	[S II]	...	...	...	...	8.2	5.0	...	...
4076	[S II]	...	...	...	...	1.5	1.7	...	...
4102	Hδ	25.7	25.9	26	26.1	28.6	26.0	26.3	26.1
4340	Hγ	47.4	46.9	49.1	47.1	47	47.0	46.5	47.1
4363	[O III]	2.9	1.9	4.8	8.1	20.5	15.8	18.4	13.8
4472	He I	...	...	...	...	3.6	3.8	...	...
4686	He II	...	...	...	...	67.6	74.3	18.3	22.7
4725	[Ne IV]	...	...	...	...	2.3	1.2	...	...
4740	[Ar IV]	...	...	...	...	6	13.7	4.1	2.2
4861	Hβ	100	100.0	100	100.0	100	100.0	100	100.0
4959	[O III]	88.4	98.5	182.4	204.0	226.2	324.2	428.9	369.2
5007	[O III]	249.2	283.9	553	587.5	651.5	934.0	1235.3	1062.5
5199	[N I]	...	...	...	...	9.4	10.1	2.2	0.9
5577	[O I]	...	...	...	...	...	...	...	...
5755	[N II]	...	...	...	...	14.4	9.0	...	...
5876	He I	14.2	13.6	23	23.4	10.6	10.2	9.8	9.2
6300	[O I]	...	...	...	...	20.2	14.8	4.9	5.1
6312	[S III]	...	...	2.4	2.3	5.8	6.6	1.8	2.5
6364	[O I]	...	...	...	...	9	4.9	3.5	1.7
6548	[N II]	13	11.9	6.9	6.0	159.4	134.4	15.7	17.2
6563	Hα	284.9	285.0	289.4	281.2	278.4	284.7	279	282.4
6584	[N II]	37.6	35.1	20.1	17.8	468.1	395.8	46.2	50.8
6678	He I	3.7	3.9	7	6.6	...	...	3.4	2.6
6717	[S II]	...	...	...	...	24.8	18.2	2.8	3.6
6731	[S II]	...	...	...	...	35.4	25.8	3.6	4.5
7006	[Ar V]	...	...	...	...	4.3	3.4	...	...
7136	[Ar III]	10.1	11.2	13.8	13.1	25.9	24.0	10.5	12.5
7320	[O II]	...	4.6	13.4	9.6	...	...	2.5	3.4
7330	[O II]	...	3.6	9	7.7	...	...	1.5	2.7
7751	[Ar III]	...	...	...	...	...	...	3.1	3.0

TABLE 3—*Continued*

λ (Å)	Line Identification	LMC-SMP 40		LMC-SMP 47		LMC-SMP 76		LMC-SMP 87	
		Observed $\log L(H\beta) = 34.33$	Model $\log L(H\beta) = 34.4$	Observed $\log L(H\beta) = 34.97$	Model $\log L(H\beta) = 35.00$	Observed $\log L(H\beta) = 34.72$	Model $\log L(H\beta) = 34.70$	Observed $\log L(H\beta) = 34.72$	Model $\log L(H\beta) = 34.70$
1239	N v	...	...	54.0	65.0	...	...	872.0	533.7
1243	N v	...	...	30.2	33.1	...	...	520.0	272.4
1336	C II	37.6	91.8	...	...	24.0	21.2	...	...
1394	Si IV	7.3	...	...	...	...	...	17.7	...
1400, 1401...	O IV	9.9	11.0	22.9	20.5	...	...	81.3	71.1
1483, 1487...	N IV]	21.6	11.9	...	88.8	...	...	756.0	672.4
1548	C IV	418.0	553.0	392.0	367.4	24.1	23.4	257.0	263.2
1551	C IV	311.0	279.0	251.0	185.0	11.8	11.8	142.0	132.6
1602	[Ne IV]	...	...	7.7	3.5	...	...	...	...
1640	He II	454.0	559.9	314.0	274.9	...	...	648.0	891.0
1661	O III]	8.6	7.1	8.0	12.7	5.6	2.7	28.4	10.4
1666	O III]	18.3	17.4	23.5	31.3	6.8	3.3	66.0	25.6
1740, 1742...	N III]	...	...	70.9	62.5	...	...	607.0	418.8
1884	Si III]	...	...	3.9	2.8	...	...	8.8	6.7
1892	Si III]	...	...	5.2	6.1	...	...	8.8	7.5
1907, 1909...	C III]	1610.0	1585.0	893.0	472.5	841.0	623.4	294.0	232.4
2139, 2143...	N II]	...	...	12.9	11.5	...	...	54.9	28.5
2321, 2325...	[O III], C II]	243.0	143.1	125.0	29.6	155.0	59.3	36.9	11.3
2424, 2436...	Ne IV]	67.5	34.7	70.3	43.0	...	...	179.0	163.7
2470	[O II]	8.9	11.0	15.0	14.2	16.2	5.4	13.9	13.2
2800	Mg II	4.5	4.8	18.9	18.8	...	...	...	...
3343	Ne V]	11.7	1.9	...	...	...	...	26.2	25.1
3426	[Ne V]	29.0	5.3	42.6	16.4	...	...	104.0	66.1
3727, 3729...	[O II]	233.5	289.9	47.8	105.2	20.6	19.7	211.0	108.4
3869	[Ne III]	105.5	117.8	125.7	129.9	8.3	8.0	122.6	157.7
3889	H, He I	...	...	22.8	26.8	32.9	31.6	26.1	18.5
3969	[Ne III], Hε	49.7	52.3	51.6	56.0	27.6	25.7	56.5	65.0
4069	[S II]	10.7	4.1	7.0	4.7	...	...	...	...
4076	[S II]	...	...	4.2	1.6	...	...	...	...
4102	Hδ	26.7	25.9	26.4	26.0	25.7	26.0	26.5	26.0
4340	Hγ	46.7	46.9	46.1	47.0	47.2	47.0	46.0	47.0
4363	[O III]	15.4	12.0	19.1	20.1	6.6	5.2	43.9	14.9
4472	He I	...	...	5.2	6.6	6.1	3.7	8.0	3.4
4686	He II	59.2	74.6	45.2	40.4	...	...	84.5	127.5
4725	[Ne IV]	...	...	3.0	0.5	...	...	...	...
4740	[Ar IV]	...	...	5.9	8.1	...	...	10.0	8.6
4861	Hβ	100.0	100.0	100.0	100.0	100.0	100.0	100.0	100.0
4959	[O III]	295.5	269.8	365.8	390.0	198.1	197.3	322.0	273.4
5007	[O III]	855.8	777.1	1053.0	1123.5	565.5	568.4	913.6	787.4
5199	[N I]	5.8	4.5	2.7	2.2	...	...	43.5	29.6
5755	[N II]	...	...	9.5	6.4	...	...	...	...
5876	He I	6.6	5.7	20.2	17.7	9.6	10.1	13.0	9.3
6300	[O I]	16.8	13.4	15.0	20.3	...	...	24.6	19.1
6312	[S III]	4.6	3.8	3.3	4.0	...	...	4.6	4.4
6364	[O I]	4.5	4.4	5.5	6.8	...	...	7.9	6.4
6435	[Ar V]	...	...	1.6	0.7	...	...	...	...
6548	[N II]	45.8	45.5	80.2	68.8	4.2	4.5	307.3	308.9
6563	Hα	279.1	286.9	276.1	284.5	281.9	283.2	269.3	284.7
6584	[N II]	137.9	133.8	238.9	202.6	12.6	13.4	921.0	909.6

TABLE 3—*Continued*

		LMC-SMP 40		LMC-SMP 47		LMC-SMP 76		LMC-SMP 87	
λ (Å)	Line Identification	Observed $\log L\,(\mathrm{H}\beta) = 34.33$	Model $\log L\,(\mathrm{H}\beta) = 34.4$	Observed $\log L\,(\mathrm{H}\beta) = 34.97$	Model $\log L\,(\mathrm{H}\beta) = 35.00$	Observed $\log L\,(\mathrm{H}\beta) = 34.72$	Model $\log L\,(\mathrm{H}\beta) = 34.70$	Observed $\log L\,(\mathrm{H}\beta) = 34.72$	Model $\log L\,(\mathrm{H}\beta) = 34.70$
6678...	He I	...	...	4.9	5.0	2.7	2.9	6.5	2.7
6717...	[S II]	15.9	16.8	6.8	5.2	...	...	22.5	11.3
6731...	[S II]	18.7	19.7	11.4	9.8	...	...	28.9	18.1
7006...	[Ar V]	...	...	2.9	1.6	...	...	3.1	1.9
7136...	[Ar III]	11.3	11.2	22.3	27.4	5.3	8.3	14.1	16.4
7237...	[Ar IV]	...	...	1.0	0.2	...	...	...	...
7320...	[O II]	7.2	8.2	11.4	10.5	4.8	4.1	5.0	4.5
7330...	[O II]	3.9	6.5	8.1	8.4	3.9	3.2	3.2	3.6
7751...	[Ar III]	...	...	...	...	...	...	3.6	4.9

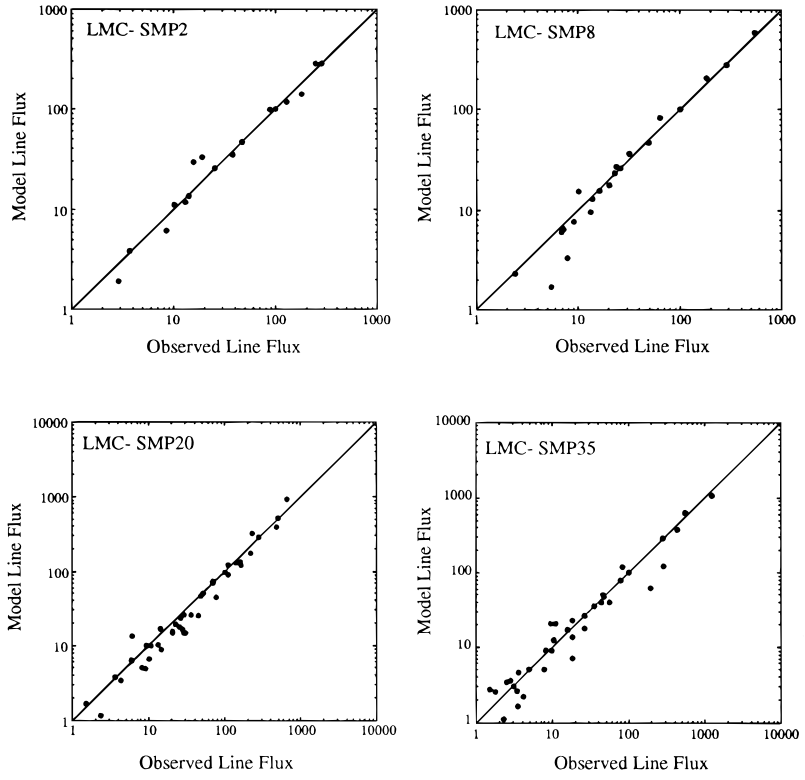

FIG. 2*a*

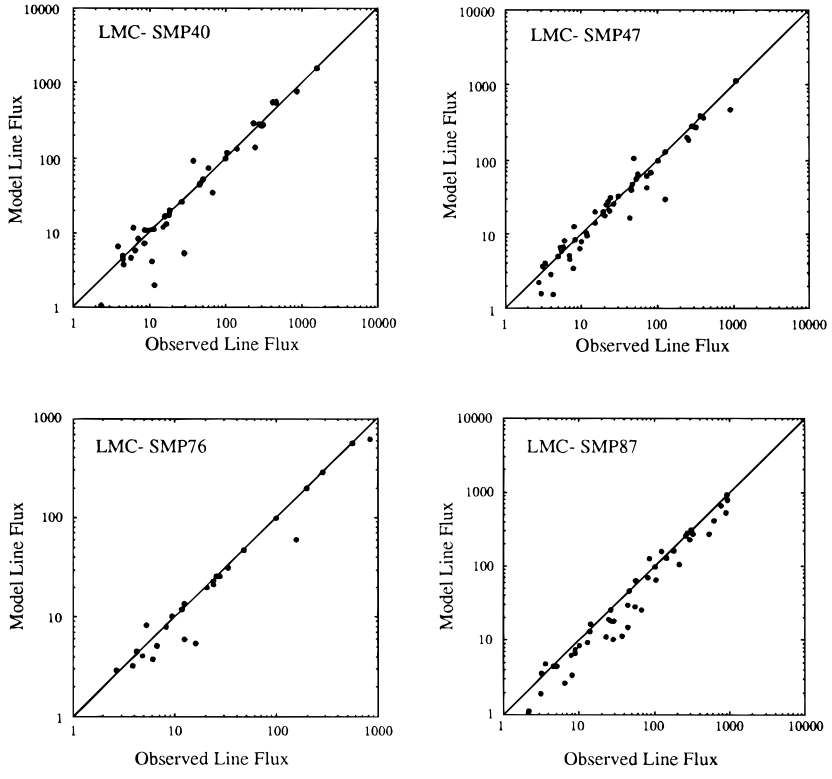

FIG. 2*b*

FIG. 2.—(*a*) The fit of the photoionization model to the observed emission-line intensities for the LMC PNs modeled in this paper. In many cases the goodness of fit is comparable with the measurement errors of the line intensities (see Meatheringham & Dopita, 1991a, 1991b). (*b*) Same as (*a*). The effect of the finite FOS aperture and its associated calibration errors is most marked in the case of LMC-SMP 87.

C IV, and [Ne V] lines all show the need for an optically thin component. However, the very strong [N I] and [O I] lines require an optically thick region with low ionization parameter illuminated by a hard photon source. The difference between the logarithmic reddening constants $c_{\rm opt}$ and $c_{\rm He\ II}$ found by Vassiliadis et al. (1996) shows that there is likely to be a calibration problem for this nebula. We believe that the measured [O II] and [Ne V] relative fluxes are overestimates. It is clear that this object has an enormous N abundance, as has been inferred by Vassiliadis et al. (1996). In

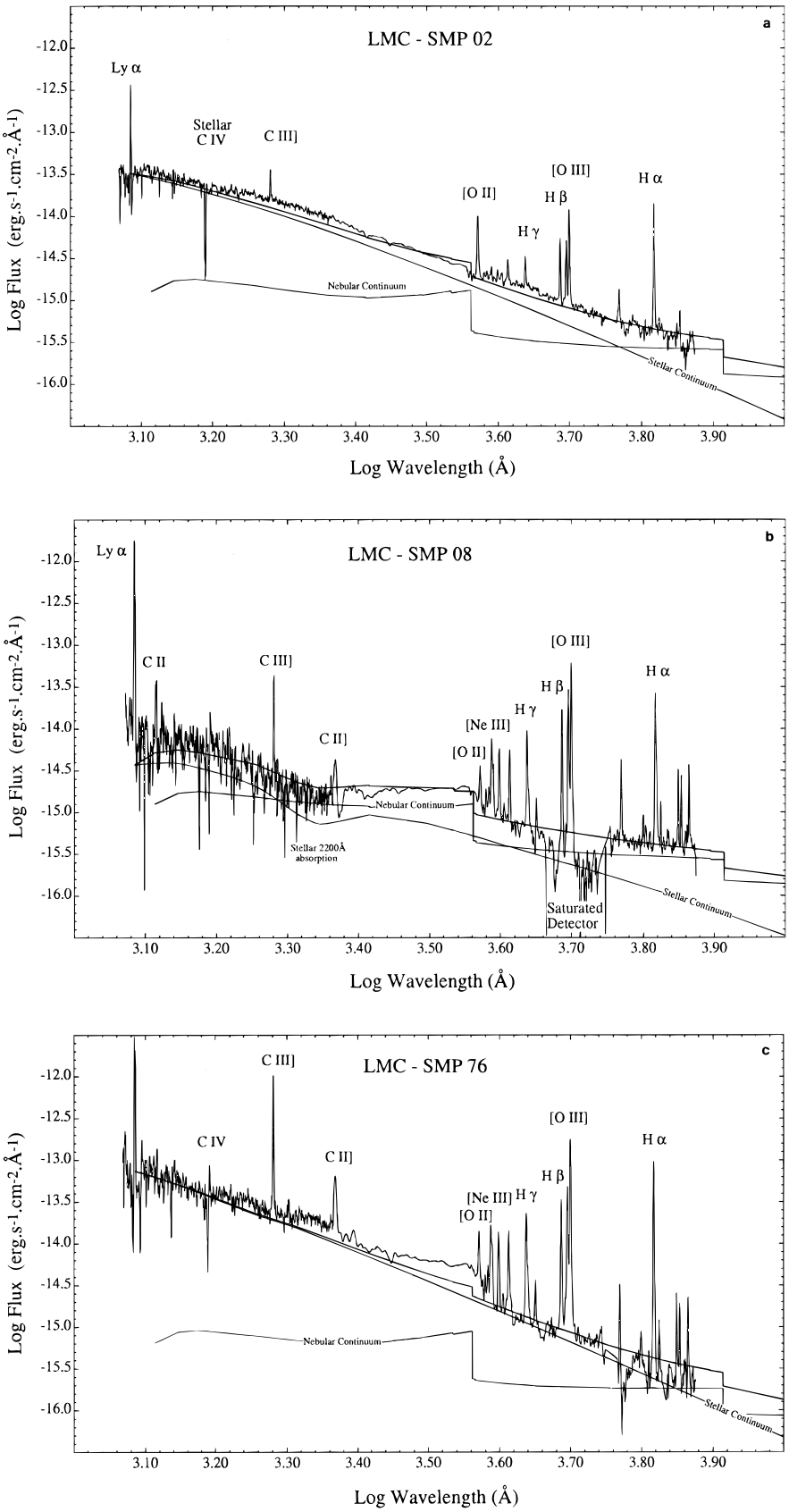

FIG. 3.—(*a*) A comparison of the observed continuum spectrum and the theoretical continuum model predicted by the photoionization model for those cases in which the central star is clearly detected. Note the very deep (100%) stellar C IV absorption feature in LMC-SMP 02. (*b*) As explained in the text, in the case of LMC-SMP 08, the central star appears to be heavily absorbed compared with the nebular, and the reddening law of the circumstellar dust displays a very deep 2200 Å feature, presumably due to C-rich grains ejected by the central star in the late AGB phase. (*c*) Same as (*a*). Note the P Cygni profile of the stellar C IV line in LMC-SMP 76.

TABLE 4

SUMMARY OF NEBULAR ABUNDANCES GIVEN WITH RESPECT TO SOLAR

Object	He	[C/H]	[N/H]	[O/H]	[Ne/H]	[Mg/H]	[Si/H]	[S/H]	[Ar/H]	[α/H]
SMP 02.....	0.102	0.01	−0.69	−0.67	−0.64	...	...	−0.61	−0.56	−0.60
SMP 08.....	0.192	−0.63	−0.57	−0.67	−0.77	...	...	−0.52	−0.52	−0.59
SMP 20.....	0.142	−1.04	0.53	−0.44	−0.35	...	−0.03	0.05	−0.22	−0.14
SMP 35.....	0.090	−0.03	−0.27	−0.55	−0.61	...	−0.77	−0.51	−0.63	−0.58
SMP 40.....	0.102	0.25	−0.26	−0.48	−0.44	−1.47	...	−0.42	−0.73	−0.51
SMP 47.....	0.172	−0.38	0.10	−0.57	−0.49	−1.38	−1.03	−0.36	−0.28	−0.37
SMP 76.....	0.076	0.48	−0.65	−0.63	−0.75	...	...	−0.61	−0.66	−0.67
SMP 83.....	0.130	−1.15	0.01	−0.31	−0.38	...	...	0.17	−0.11	−0.05
SMP 85.....	0.105	0.18	−0.42	−0.53	−0.61	...	...	−0.91	−0.32	−0.55
SMP 87.....	0.176	−0.66	0.90	−0.37	−0.19	...	−0.65	−0.10	−0.38	−0.21

our modeling, we have adopted an isochoric density model for zone 2, but the density of this region is not well defined by the observations.

3. DISCUSSION

3.1. *Masses of Central Stars*

The photoionization modeling presented here and in Papers I and II has allowed us to place accurately the PN central stars onto the theoretical [log $(L/L_\odot)$:log $(T_{\rm eff})$] Hertzsprung-Russell (H-R) diagram. We can, therefore, use the Vassiliadis & Wood (1993) evolutionary models to determine both the current core mass and the original mass of the central star. This analysis depends upon whether the central star leaves the AGB as a H- or an He- burning object, since this affects radically the subsequent evolution, both in the rate of evolution across the H-R diagram, and in the position of the central star on the H-R diagram. In Paper IV, we had attempted to sort the central stars according to their dynamical evolution, demanding that the dynamical ages be consistent with the theoretical evolutionary age. With the improved determination of the stellar log $(L/L_\odot)$ and log $(T_{\rm eff})$ given by these models, we can now eliminate the ambiguities, so that all except LMC-SMP 85 can now be assigned definite classification as either H or He burners. The types that we have assigned are given in Table 5. In Figure 4 we show the theoretical H-R diagrams for both H and He burners from Vassiliadis & Wood (1993), with the inferred locations of the LMC PNs.

The initial mass–core mass relationship is critical to the interpretation of these results. This is determined essentially by the mass loss on the giant and AGB phases, which channels a wide range of initial stellar masses into a narrow range of core mass. The mass-loss formulation adopted by Vassiliadis & Wood (1993) and used by Marigo, Bressan, & Chiosi (1996) is to be preferred, since this ensures that the models match the period-luminosity relationship of the long-period variables, the maximum luminosity of the AGB stars, and the bolometric luminosity distribution of the carbon stars observed in the LMC. Combining the results of these two papers, we find that the relationship between initial mass, M, and final core mass, $M_{\rm core}$, can be expressed as

$$(M_{\rm core}/M_\odot) = 0.5241 + 0.0438(M/M_\odot) + 0.00949(M/M_\odot)^2 \ . \quad (3.1)$$

This expression fits the models to better than 0.01 $M_\odot$ throughout the range. We also fit the Vassiliadis & Wood (1993) models to smooth functions of the H-burning and He-burning lifetimes, to give the age of the star in terms of its mass by

$$(\tau/{\rm Gyr}) = 11[M/M_\odot]^{-3.1} + 0.46[M/M_\odot]^{-4.6} \ . \quad (3.2)$$

We have used Figure 4 and equations (3.1) and (3.2) to derive the initial mass, core mass, and age of each PN. These are also given in Table 5. Because of the extreme nonlinearity of parameters, and the dependence on location of the PNs on the H-R diagram, full measurement errors are given.

3.2. *Chemical Evolution History of the LMC*

Kaler & Jacoby (1990, 1991) and Jacoby & Kaler (1993) had already shown that there is a relationship between core mass and He and N abundance. However, it is difficult to separate changes in abundance of elements affected by dredge-up processes from the changes in abundance produced by the chemical evolution over time. Tables 4 and 5 show that, with these new data, we can now distinguish a core mass:metallicity or, equivalently, an age:metallicity relationship for the LMC using [α/H] as a metallicity indicator on the grounds that this is little affected by dredge-up.

TABLE 5

DERIVED PARAMETERS OF THE PN CENTRAL STARS[a]

Object	log $(L/L_\odot)$	log $(T_{\rm eff})$ (K)	Type	Core Mass $(M_\odot)$	Initial Mass $(M_\odot)$	Age (Gyr)
SMP 02.....	3.128	4.591	He	0.571(+0.006 −0.002)	0.90(+0.08 −0.03)	12.2–17.8
SMP 08.....	3.594	4.716	He	0.600(+0.006 −0.005)	1.35(+0.08 −0.08)	3.7–5.4
SMP 20.....	3.519	5.179	H	0.604(+0.007 −0.007)	1.40(+0.10 −0.10)	3.2–5.0
SMP 35.....	3.381	5.033	He	0.590(+0.021 −0.013)	1.20(+0.30 −0.15)	3.2–9.8
SMP 40.....	3.124	5.246	H	0.634(+0.016 −0.008)	1.80(+0.20 −0.10)	1.30–2.16
SMP 47.....	3.677	5.149	H	0.618(+0.016 −0.011)	1.60(+0.20 −0.15)	1.81–3.56
SMP 76.....	3.735	4.763	H	0.590(+0.010 −0.010)	1.20(+0.15 −0.15)	4.5–9.8
SMP 83.....	4.431	5.230	He	0.980(+0.15 −0.13)	5.00(+1.0 −1.0)	0.04–0.15
SMP 85.....	3.857	4.653	He	0.650(+0.05 −0.02)	2.00(+0.60 −0.20)	0.57–1.8
			H	0.614(+0.020 −0.014)	1.55(+0.25 −0.15)	1.9–4.0
SMP 87.....	3.690	5.225	He	0.693(+0.014 −0.018)	2.50(+0.15 −0.20)	0.54–0.84

[a] The type of SMP 85 remains ambiguous.

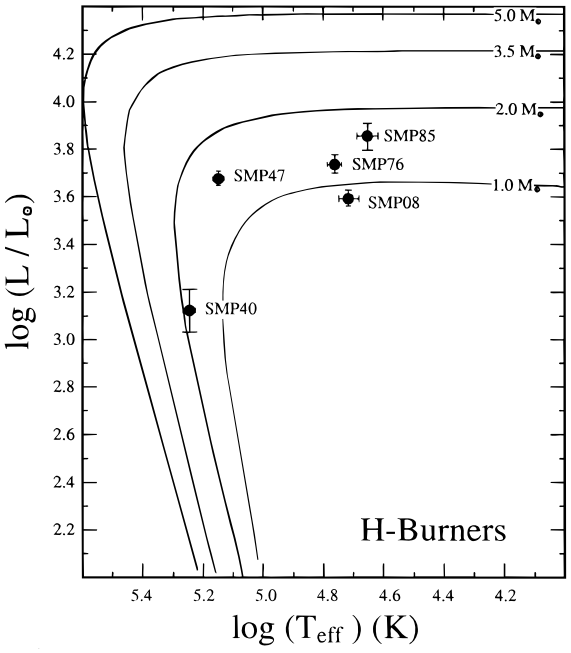

FIG. 4a

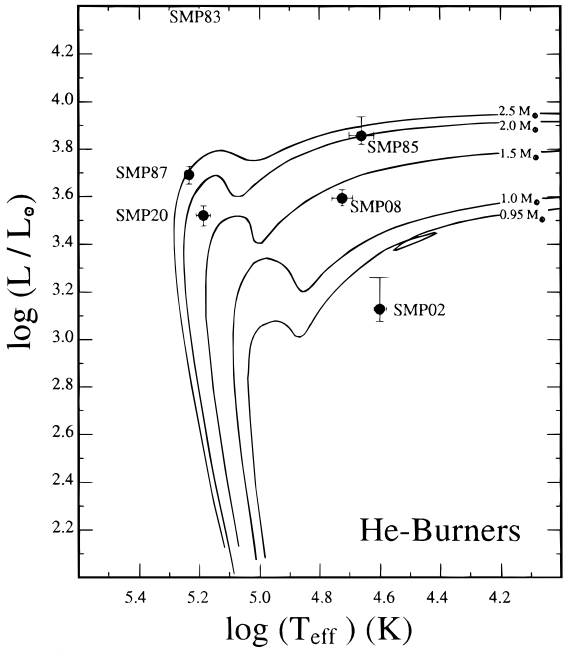

FIG. 4b

FIG. 4.—(*a*) The location on the H-R diagram of PN central stars for those objects identified as having left the AGB as H burners. The theoretical tracks are from Vassiladis & Wood (1993). The 1.0 $M_{\odot}$ track is for SMC rather than LMC abundances. (*b*) Same as (*a*), but for the He burners.

These relationships are shown in Figures 5*a* and 5*b*. Because of the highly nonlinear relationship between core mass and age, the resolution of the age becomes progressively poorer as we go back in time, so the age axis is plotted on a logarithmic scale. Despite the relatively few number of points, Figure 5 reveals that in the LMC there was a long period of quiescence between ~15 Gyr and ~4 Gyr ago, during which the metallicity remained close to SMC values. There is no evidence in this sample of any "halo" abundance objects. About 1–3 Gyr ago, there appears to have been a strong burst of star formation that more than doubled the metallicity. In recent times, star formation and the rate of chemical evolution slowed again.

This is in remarkable agreement with the data on both field stars and clusters. From color-magnitude diagrams of the field stars (Hardy et al. 1984; Frogel & Blanco 1983; Butcher 1977; Stryker 1983, 1984), show that in the region of the bar of the LMC, most of the star formation occurred in a major burst ~3 Gyr ago and continued at a lower rate until ~0.1 Gyr ago. The latest cluster data (Girardi et al. 1995) show a long period of quiescence, followed by a large rate of cluster formation 1–2 Gyr ago with a secondary peak at ~0.1 Gyr. The "age gap" 3–12 Gyr ago, and a rapid increase in metallicity 2–3 Gyr ago, is also seen in the color-magnitude diagrams of individual clusters (Costa 1991). Finally, recent *HST* data on the distribution of stars in the color-magnitude diagram for a field in the outer disk of the LMC (Gallagher et al. 1996) shows that there was a strong burst in star formation ~2.3 Gyr ago. During this burst, the star formation rate was enhanced by *at least* a factor of 3, and possibly by as much as a factor 50.

Clearly, the results presented here show the great potential offered by the PNs in the investigation of the chemical history of the LMC. Figure 5 should be much improved when the results of cycles 4–6 are available.

3.3. *The Refractory Elements*

From Tables 2 and 4, we see that abundances of Mg are determined in two objects, and Si abundances are estimated for four objects altogether. The LMC current interstellar abundances derived by Russell & Dopita (1990, 1992) are also given in Table 2. In that work, the Mg abundances were determined from supergiant atmospheres, and the Si abundance was determined from both supergiants and from energetic supernova remnants, in which refractory grains are expected to have been destroyed by sputtering (Draine 1995).

By inspection, it is clear that Mg is depleted in the ionized gas by ~1.3 dex, and Si by ~1.1 dex, apart from LMC-SMP 20. Since both Mg and Si are elements produced by the α-process, and they are essentially unaffected by dredge-up processes occurring during the giant and the AGB phases of evolution, we would expect that the abundances of these elements in the material ejected by the central star would reflect those of the star at the time of its formation. This result demonstrates, therefore, that both Mg and Si are depleted onto refractory grain materials, presumably silicates, which are not destroyed by the UV field of the central star over the evolutionary lifetime of the PN. In this regard, it is significant that the four objects in which Si III] lines are seen are all hot type PNs. We would expect that conditions in these objects would lead to significant photodestruction of grains.

In the local interstellar medium, the observed depletions of refractory elements are tightly correlated with the average value of the neutral hydrogen density. In cold dense clouds, both Mg and Si are depleted by 1.0 dex or more (Jenkins, Savage, & Spitzer 1986; Joseph 1988). However, in the diffuse interstellar medium (ISM), Mg is almost undepleted. This effect seems to be correlated with grain destruction by shocks in the diffuse ISM. Gondhalekar (1984) has shown that significant shock processing occurs in high-velocity gas, and even at velocities as low as 50 km s^{-1}, at least 10% of the Si is returned to the ISM. It is interesting to note that this velocity is lower than the observed expansion velocities of both LMC-SMP 40 and LMC-SMP 47, both

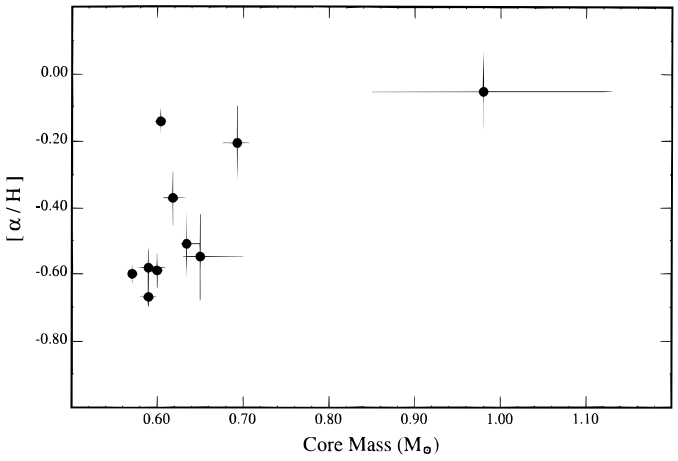

FIG. 5*a*

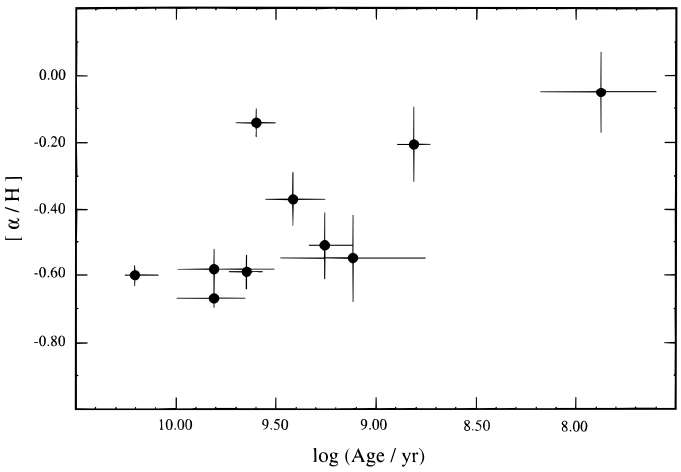

FIG. 5*b*

FIG. 5.—(*a*) Core mass:age and (*b*) the metallicity:age relationship inferred from the LMC PNs. Errors in the determination of the core mass, and hence of the initial mass, lead to fairly substantial errors in the determination of ages and loss or resolution in time at early epochs. Nonetheless, the main features of the chemical evolution history can be clearly distinguished; a long period of quiescence, followed by a short period of activity within the past 3 Gyr, which more than doubled the base metallicity of the LMC. Evidence of a burst of star formation and rapid enrichment at this time is also found in the study of color:magnitude arrays of clusters and field stars (see text).

of which display large depletions in the refractory elements. This seems to require that the gas currently in the ionized gas has passed through an ionization front and has been subsequently accelerated up to the observed expansion velocity, rather than being shocked directly up to this velocity. This picture is consistent with our dynamical model, presented above.

3.4. *The α-Process Elements*

The chemical enrichment of the α-process elements should be essentially unaffected by the dredge-up processes discussed in the following section. This is confirmed by Figure 6, in which we have plotted the abundances of the individual α-process elements against the mean; ([Ne/H] + [S/H] + [Ar/H])/3. The line shown is the two-dimensional mean square best fit. Correlation coefficients vary between 0.66 (Ar) and 0.83 (S). The slope of the (O:α) fit is appreciably less than 1 (0.56), and that of the (S:α) fit is appreciably greater than unity (1.51).

The result for O may be marginal evidence for O-N processing, but if so, this is occurring at a much lower rate than suggested by Dopita & Meatheringham (1991b). As for S, there is no known dredge-up process that could cause this effect. However, it is significant that the derived S abundance relies heavily on the optical [S II] lines. In our spectrophotometry, the only other S line seen frequently is the (temperature-sensitive) [S III] λ6312 line. Thus, sulfur is not seen in its dominant ionization stage, and systematic errors in the abundance determination may occur. Many of the objects showing high apparent S abundance are high-excitation objects. In these objects, much of the [S II] line intensity arises in a partially ionized zone ionized by the hardest photons. Petuchowski & Bennett (1995) made a convincing case that a significant fraction of [S II] emission in such regions can arise by direct photoionization to excited states by the diffuse stellar continuum below 912 Å. This process of line emission has not so far been included in MAPPINGS II (despite the fact that photoionization to excited states has long been included in the photoionization rate calculations), and it could lead to a systematic overestimate of the S abundance in high-excitation objects.

3.5. *Mass Dependence of Chemical Dredge-up in the LMC*

The chemical evolution of the material that is ejected as a PN shell is determined by three major dredge-up episodes and by "hot-bottom" burning (Iben & Renzini 1983; Renzini & Voli 1981) summarized as follows:

1. The first dredge-up, operating as the star becomes a red giant for the first time, is produced by the penetration of the convective envelope into regions that are partially CNO burned. The dredged-up material is mixed throughout the envelope, with enhancement of the ^{13}C and ^{14}N abundances and a decrease in ^{12}C abundance.
2. The second dredge-up appears in the early AGB evolution of stars more massive than 3–5 $M_{\odot}$, when the hydrogen-burning shell extinguishes, and once again the base of the convective envelope dips into burned material. Envelope enhancements of ^{4}He, ^{14}N, and ^{13}C are produced.
3. The third dredge-up occurs in the thermally pulsing AGB phase in which, after each He-burning pulse, the convective envelope dips down, dredging up nuclear processed material rich in ^{4}He, ^{12}C, and the *s*-process elements.
4. Hot-bottom burning occurs in the more massive AGB stars ($M > 3\ M_{\odot}$) when convection in the stellar envelope cycles matter through the hydrogen-burning shell during the interpulse phase, with resultant partial CNO cycling of the whole envelope. Significant ^{14}N, and possibly ^{4}He, production may occur.

These processes are expected to be dependent upon both mass and initial metallicity of the star.

In Figure 7, we show the abundances of elements likely to be affected by dredge-up and hot-bottom burning (He, C, and N) as a function of the abundance of the α-process elements, as defined in the previous sections. Thanks to the metallicity-age relation, the axis is a measure of both initial metallicity and of mass of the central star.

We find a striking and systematic trend with very little scatter in the abundances of He, C, and N with α-process abundance and/or mass. The effect of the second dredge-up is apparent at intermediate masses through the enhancement of He. The enhancement of C at the low mass/

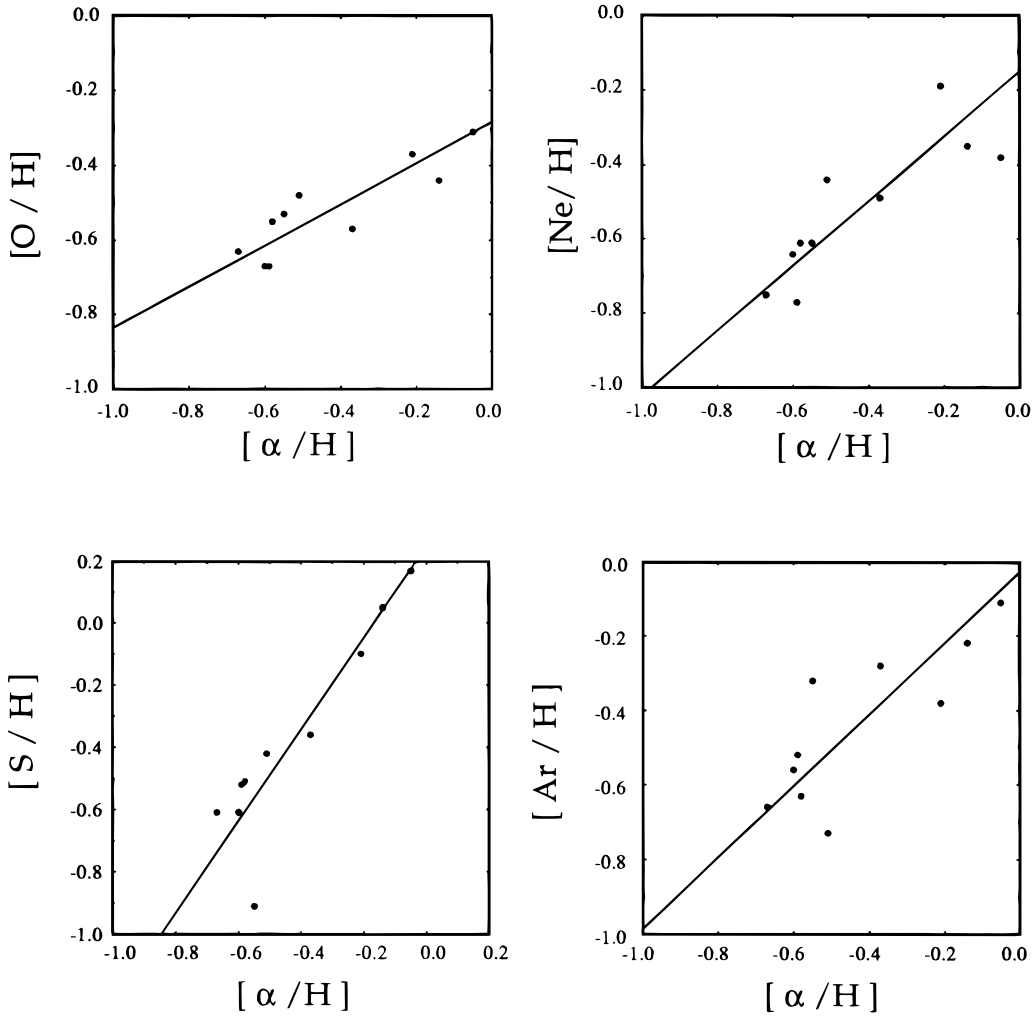

FIG. 6.—Metallicity-metallicity plots for the α-process elements. Relative abundances are normalized to solar values, following the convention used in stellar abundance analyses. There is no evidence for a contribution to Ne through dredge-up of ^{22}Ne, but the slope of the correlation with O is appreciably less than the average, while the slope of the S metallicity-metallicity relationship is steeper than the average.

abundance end indicates that the third dredge-up of C is important for such stars in the LMC, as is well known from studies of carbon stars. An important new result is that the sum of the C + N abundances shows little systematic trend, in agreement with Kaler & Jacoby (1990, 1991). This indicates that the third dredge-up is significant at all masses. In stars of higher mass and/or abundance, hot-bottom burning appears to be operating efficiently to produce the very high N abundances observed, with much of the dredged-up C converted to N.

In Figure 8, we compare the measured He/H abundance as a function of stellar mass (see § 3.1) with the results of Marigo et al. (1996) for LMC abundances. It should be remarked at the outset that such a direct comparison is not exactly fair, since we have shown in § 3.2 that the use of a constant initial abundance is invalid because of the metallicity:age relationship in the LMC. The effect of the lower initial abundance in the older, low-mass stars is to make the third dredge-up operate much more efficiently, increasing the C/O ratio (Wood 1981). The observed amount of He increase is about 2.5 times that predicted for masses in the range 2–3 $M_{\odot}$. The models need to produce more helium either by more second dredge-up or more hot-bottom burning. If the latter case prevails, a very high N enhancement would be expected to accompany the He enhancement.

The top panel of Figure 9 plots N/O against He/H for the observed LMC PNs and the models of Marigo et al. (1996). From this plot, and Figure 13 of Marigo et al. (1996), it is clear that high He/H is generally associated with high N/O, indicating that hot-bottom burning plays a more important role in intermediate mass stars than current models suggest.

Figure 9 also compares the C/O abundance ratio with the theoretical predictions. The agreement is again poor. For masses greater than $\sim 2\ M_{\odot}$, the C/O (and N/O) versus He/H plot would be brought into much better agreement with observation if hot-bottom burning were operating in the models, increasing envelope He while at the same time decreasing envelope C/O (and increasing N/O). As a final point, we note that the PNs associated with the lowest mass progenitors have C/O ratios much larger than the models, showing that the third dredge-up remains more important to lower masses than current theory predicts.

The enhancement of Ne predicted by the theoretical models of Marigo et al. (1996) is not seen at all (Figure 9). This enhancement is in the form of ^{22}Ne and is produced from ^{14}N via the chain ^{14}N(α, γ) ^{18}F(β^+, ν) ^{18}O(α, γ) ^{22}Ne. Marigo et al. (1996) assume, following Boothroyd & Sackmann (1988), that essentially all ^{14}N left over from the CNO cycle is converted through to ^{22}Ne in a helium shell flash. They assume also, following Gallino et al. (1988), that the conversion of ^{22}Ne to ^{25}Mg via the neutron source reaction

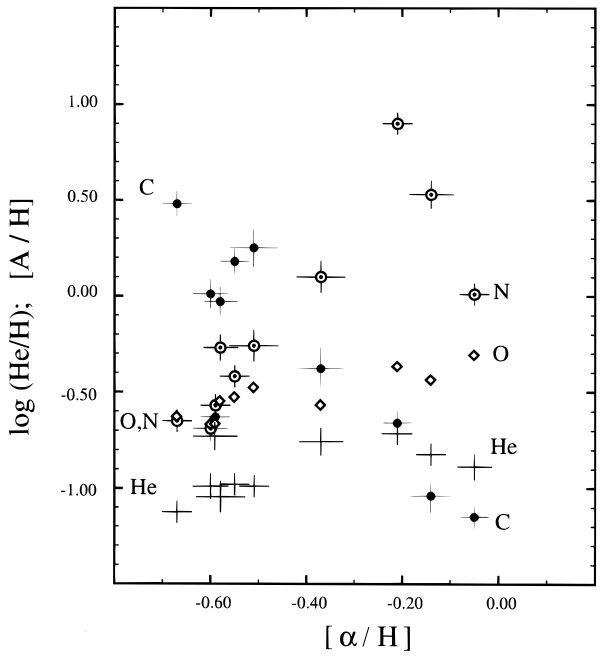

FIG. 7.—The variation of He, C, N, and O abundances with the abundance of the heavier α-process elements: [α/H] = ([Ne/H] + [S/H] + [Ar/H])/3. Error bars have been omitted for O to increase clarity, but they are similar to those of C and N. As discussed in the text, the *x*-axis can be interpreted as a mass sequence. This figure shows the systematic dependence of dredge-up processes on mass and metallicity.

^{22}Ne(α, n)^{25}Mg is very low at low core masses. The lack of ^{22}Ne we observe would require, on the contrary, almost complete conversion of ^{22}Ne to ^{25}Mg. However, there are two problems with this suggestion. First, the depletion factor for Mg would have to be much larger than what we estimated in § 3.3 above and, second, the observed isotopic ratios of ^{24}Mg, ^{25}Mg, and ^{26}Mg in thermally pulsing AGB stars do not show any evidence for the dredge-up of ^{25}Mg (Smith & Lambert 1986). The observational evidence therefore suggests that the reaction sequence ^{14}N(α, γ) ^{18}F(β^+, ν) ^{18}O(α, γ) ^{22}Ne(α, n) ^{25}Mg must stop before significant amounts of Ne or Mg are produced. But the sequence

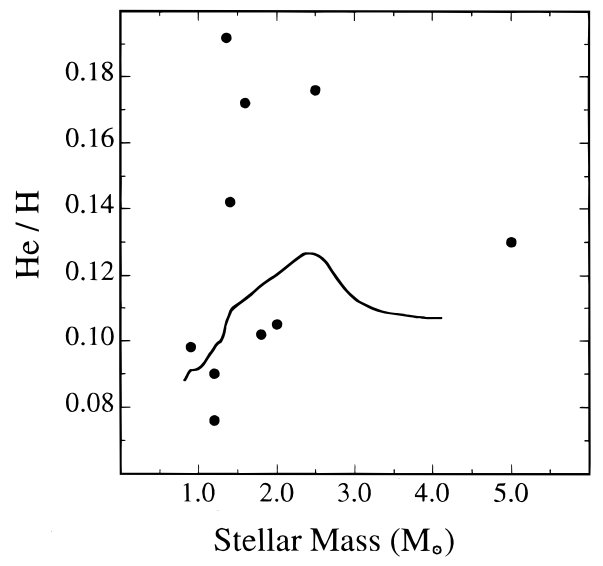

FIG. 8.—Variation of the helium abundance with initial mass of the central star. The curve is from Marigo et al. (1996). Clearly, much more dredge-up is occurring than is predicted by the theoretical models.

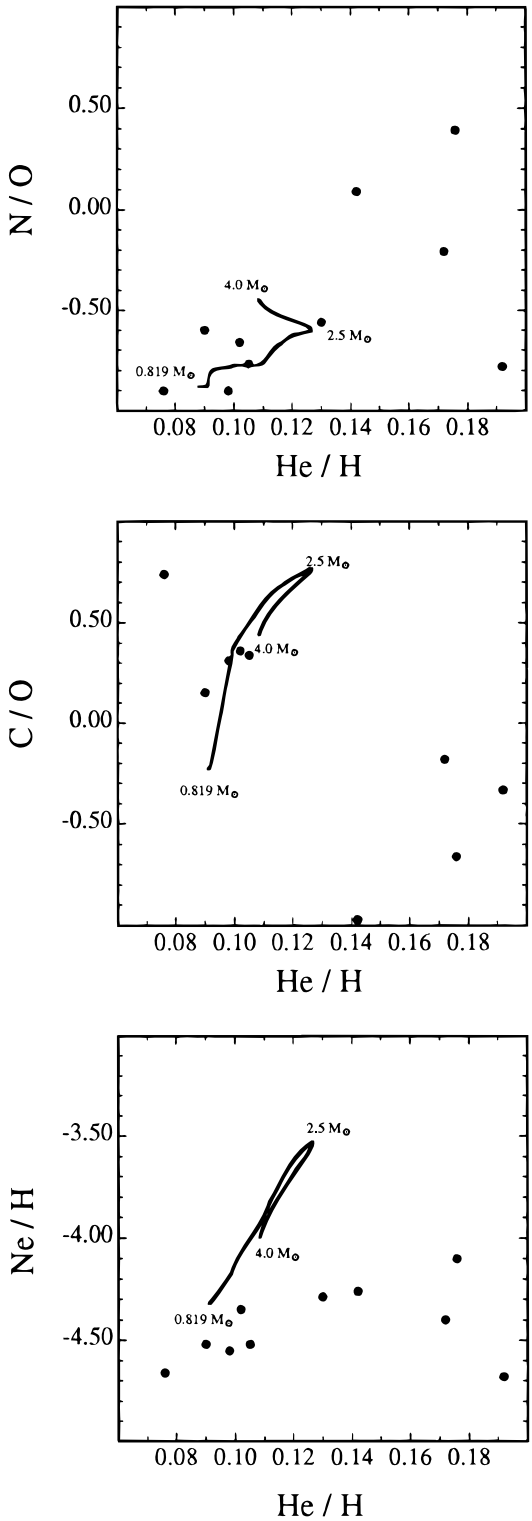

FIG. 9.—The variation of the relative abundances of He, C, N, and O compared with the helium abundance for the LMC PNs. The curves are from Marigo et al. (1996). The large differences between theory and observation are discussed in the text.

cannot stop at ^{18}O either, since thermally pulsing AGB stars do not show evidence for enhancements in ^{18}O (Smith & Lambert 1990). On the other hand, current reaction rate estimates have the reactions ^{14}N(α, γ) ^{18}F(β^+, ν) ^{18}O occurring early in each helium shell flash. The final products of the ^{14}N + α reaction are clearly not identified at the present time.

4. CONCLUSIONS

The results presented in this paper have demonstrated the utility of *Hubble Space Telescope* UV and ground-based optical spectrophotometry in the analysis of the evolution of planetary nebulae in the Magellanic Clouds, in examining the mass dependence of dredge-up processes, and in inferring details of the star formation history of the Magellanic Clouds. We have been able to place the central stars on the H-R diagram and so determine core masses and (via theoretical tracks) infer the initial masses and ages of 10 objects.

The observed abundance patterns are qualitatively consistent with the (mass-dependent) operation of the various chemical dredge-up processes as predicted by theory. Dredge-up of C during the thermal pulsing stage appears to be most important, and "hot-bottom burning" transforms much of this C to N in the more massive stars. There is no sign of dredge-up of ^{22}Ne. It is clear that, although useful for qualitative descriptions of the dredge-up processes, current theoretical models are very inadequate for the task of describing these processes in detail. The observations presented here provide an important constraint on future theoretical models. By the time our *HST* program is complete, we will have data of similar quality on a further 20 or so LMC PNs, and for at least 10 SMC PNs. Therefore, we expect to be able to determine the effect of lower metallicity on these dredge-up processes, refine our understanding of dredge-up processes in LMC PNs, and infer details of the metallicity history of the SMC at about the same resolution the results for the LMC presented in this paper.

The observed spread in the α-process element abundances can be understood as being due to differences in core mass of the PNn, which is directly related to initial mass of the precursor star. On this basis, we have derived the chemical history of the LMC. This is the first time that data derived from PNs have been used in this way. We find that the base metallicity of the LMC almost doubled $\sim$2 Gyr ago. This is consistent with studies of field stars and of clusters, which show that there was a major burst of star formation at that time. It is also consistent with the mean kinematic age of the PN population derived by Meatheringham et al. (1988a).

The results presented here are based on observations with the NASA/ESA *Hubble Space Telescope*, obtained at the Space Telescope Science Institute, which is operated by the Association of Universities for Research in Astronomy, Inc., under NASA contract NAS 5-26555. Support for this work was provided by NASA through grant number GO-2266 from the Space Telescope Science Institute. Australian collaborators wish to acknowledge travel and publication support under a major grant from the International Science and Technology Division of the (Australian) Department of Industry, Science, and Technology. The authors would particularly like to thank the referee, George Jacoby, for his careful reading of the manuscript and his suggestions which both improved the end product for the reader and prevented the propagation of careless errors in to print.

REFERENCES

Alongi, M., Bertelli, G., Bressan, A., Chiosi, C., Fagotto, F., Greggio, L., & Nasi, E. 1993, A&AS, 97, 851
Anders, E., & Grevesse, N. 1989, Geochim. Cosmochim. Acta, 53, 197
Barlow, M. 1989, in IAU Symp. 131, Planetary Nebulae, ed. S. Torres-Peimbert (Dordrecht: Kluwer), 319
Binette, L., Dopita, M. A., & Tuohy, I. R. 1985, ApJ, 297, 476
Boothroyd, A. I., & Sackman, I.-J. 1988, ApJ, 328, 653
Bressan, A., Fagotto, F., Bertelli, G., & Chiosi, C. 1993, A&AS, 100, 647
Butcher, H. R. 1977, ApJ, 216, 372
Caldwell, J., & Laney, C. D. 1991, in IAU Symp. 148, The Magellanic Clouds, ed. R. Haynes & D. Milne (Dordrecht: Reidel), 249
Chiosi, C., & Marigo, P. 1996, A&A, in press
Da Costa, G. S. 1991, in IAU Symp. 148, The Magellanic Clouds, ed. R. Haynes & D. Milne (Dordrecht: Kluwer), 183
Dopita, M. A. 1993, in IAU Symp. 155 Planetary Nebulae, ed. R. Weinberger & A. Acker (Dordrecht: Kluwer), 433
Dopita, M. A., Ford, H. C., Bohlin, R. C., Evans, I. N., & Meatheringham, S. J. 1993, ApJ, 418, 804 (Paper I)
Dopita, M. A., Ford, H. C., Lawrence, C. J., & Webster, B. L. 1985, ApJ, 296, 390
Dopita, M. A., Ford, H. C., & Webster, B. L. 1985, ApJ, 297, 593
Dopita, M. A., & Meatheringham, S. J. 1991a, ApJ, 367, 115
———. 1991b, ApJ, 377, 480
Dopita, M. A., Meatheringham, S. J., Ford, H. C., & Webster, B. L. 1988, ApJ, 327, 651
Dopita, M. A., et al. 1996, ApJ, 460, 320 (Paper IV)
———. 1994, ApJ, 426, 150 (Paper II)
Draine, B. T. 1995, Ap&SS, 233, 111
Fitzpatrick, E. L. 1985, ApJ, 299, 219
Frogel, J. A., & Blanco, V. C. 1983, ApJ, 274, L57
Gallagher, J. S., et al. 1996, ApJ, 466, 732
Gallino, R., Busso, M., Piccio, G., Raiteri, C. M., & Renzini, A. 1988, A&AS, 104, 365
Girardi, L., Chiosi, C., Bertelli, G., & Bressan, A. 1995, A&A, 298, 87
Gondhalekar, P. M. 1984, in RAL Workshop, Gas in the Interstellar Medium (SERC:RAL-84-101), 66
Hardy, E., Buonanno, R., Corsi, C., Janes, K., & Schommer, R. 1984, ApJ, 278, 592
Hoyle, F., & Wickramasinghe, N. C. 1991, The Theory of Cosmic Grains (Dordrecht: Kluwer)
Iben, I., Jr., & Renzini, A. 1983, A&A, 21, 271
Jacoby, G. H., Ciardullo, R., & Walker, A. R. 1990, ApJ, 365, 471
Jacoby, G. H., & Kaler, J. B. 1993, ApJ, 417, 204
Jenkins, E. B., Savage, B. D., & Spitzer, L. 1986, ApJ, 301, 355
Joseph, C. L. 1988, ApJ, 335, 157
Kaler, J. B. 1976, ApJ, 210, 843
Kaler, J. B., & Jacoby, G. H. 1990, ApJ, 362, 471
———. 1991, ApJ, 382, 134
Kwok, S., Purton, C. R., & Fitzgerald, P. M. 1978, ApJ, 219, L125
Marigo, P., Bressan, A., & Chiosi, C. 1996, A&A, in press
Meatheringham, S. J., & Dopita, M. A. 1991a, ApJS, 75, 407
———. 1991b, ApJS, 76, 1085
Meatheringham, S. J., Dopita, M. A., Ford, H. C., & Webster, B. L. 1988a, ApJ, 327, 651
Meatheringham, S. J., Dopita, M. A., & Morgan, D. H. 1988b, ApJ, 329, 166
Panagia, N., Gilmozzi, R., Macchetto, F., Adorf, H.-M., & Kirshner, R. P. 1991, ApJ, 380, L23
Peimbert, M. 1995, in STScI Symp. Ser. 8, The Analysis of Emission Lines, ed. R. E. Williams & M. Livio (Cambridge: Cambridge Univ. Press), 165
Petuchowski, S. J., & Bennett, C. L. 1995, ApJ, 438, 735
Priete-Martinez, A., & Pottasch, S. R. 1983, A&A, 126, 31
Ratag, M. A. 1991, Ph.D. thesis, Univ. Gröningen
Renzini, A., & Voli, M. 1981, A&A, 94, 175
Russell, S. C., & Dopita, M. A. 1990, ApJS, 74, 93
———. 1992, ApJ, 384, 508
Sanduleak, N., MacConnell, D. J., & Davis Philip, A. G. 1978, PASP, 90, 621
Schönberner, D. 1983, ApJ, 272, 708
Seaton, M. J. 1979, MNRAS, 187, 73
Smith, V. V., & Lambert, D. L. 1986, ApJ, 311, 843
———. 1990, ApJS, 72, 387
Stoy, R. H. 1933, MNRAS, 93, 588
Stryker, L. L. 1983, ApJ, 266, 82
———. 1984, ApJS, 55, 127
Sutherland, R. S., & Dopita, M. A. 1993, ApJS, 88, 253
Vassiliadis, E., et al. 1996, ApJS, 105, 375 (Paper III)
Vassiliadis, E., & Wood, P. R. 1993, ApJ, 413, 641
Wiedemann, V. 1987, A&A, 188, 74
Wood, P. R. 1981, ApJ, 281, 311
Wood, P. R., Arnold, A., & Sebo, K. 1996, in preparation
Wood, P. R., Bessell, M. S., & Dopita, M. A. 1986, ApJ, 311, 632
Wood, P. R., Meatheringham, S. J., Dopita, M. A., & Morgan, D. H. 1987, ApJ, 320, 178